COMPLEX SYSTEM MODELING AND SIMULATION
ISSN 2096-9929 03/06 pp 307−321
Volume 2, Number 4, December 2022
DOI: 10.23919/CSMS.2022.0019

Brain-Controlled Multi-Robot at Servo-Control Level Based on Nonlinear Model Predictive Control

Zhenge Yang, Luzheng Bi*, Weiming Chi, Haonan Shi, and Cuntai Guan

Abstract: Using a brain-computer interface (BCI) rather than limbs to control multiple robots (i.e., brain-controlled multi-robots) can better assist people with disabilities in daily life than a brain-controlled single robot. For example, one person with disabilities can move by a brain-controlled wheelchair (leader robot) and simultaneously transport objects by follower robots. In this paper, we explore how to control the direction, speed, and formation of a brain-controlled multi-robot system (consisting of leader and follower robots) for the first time and propose a novel multi-robot predictive control framework (MRPCF) that can track users' control intents and ensure the safety of multiple robots. The MRPCF consists of the leader controller, follower controller, and formation planner. We build a whole brain-controlled multi-robot physical system for the first time and test the proposed system through human-in-the-loop actual experiments. The experimental results indicate that the proposed system can track users' direction, speed, and formation control intents when guaranteeing multiple robots' safety. This paper can promote the study of brain-controlled robots and multi-robot systems and provide some novel views into human-machine collaboration and integration.

Key words: brain-computer interface; human-machine collaboration; model predictive control; multi-robot system

1 Introduction

With the constant progress of science and technology, the quality of life of people has increasingly improved. However, society is also facing the problem of increasing population aging. Moreover, the number of patients with motor dysfunction increases. Paralysis, amputation, and loss of central nervous system function caused by these diseases or other reasons make patients often need the care of others in their daily lives, which brings heavy pressure and burden to patients, their families, and society. Therefore, it is pretty meaningful to develop a technology that can improve the self-care ability of these people.

Brain-computer interfaces (BCIs) have been developed to address the above-mentioned living problems for disabled people. BCIs can provide a direct communication channel between the human brain and physical devices via interpreting users' brain signals into commands[1]. This new interactive method brings new ideas and technologies to help disabled patients and has broad application prospects.

A brain-controlled mobile robot was first put forward in 2004[2]. Since then, more and more researchers have devoted themselves to promoting its development, and brain-controlled mobile robots have continued to progress. At the initial stage, researchers focused on building a brain-controlled robot via a BCI to interpret brain signals into commands to control a robot directly. The class of brain-controlled robots is called direct-brain-control robots. Tanaka et al.[3] put forward a brain-controlled wheelchair in 2005, and the subjects

• Zhenge Yang, Luzheng Bi, Weiming Chi, and Haonan Shi are with the School of Mechanical Engineering, Beijing Institute of Technology, Beijing 100081, China. E-mail: 3120215258@bit.edu.cn; bhxblz@bit.edu.cn; chiwm123@163.com; 1075216424@qq.com.
• Cuntai Guan is with the School of Computer Science and Engineering, Nanyang Technological University, Singapore 639673, Singapore. E-mail: ctguan@ntu.edu.sg.
* To whom correspondence should be addressed.
Manuscript received: 2022-09-07; revised: 2022-09-19; accepted: 2022-09-24

can generate commands to control the wheelchair direction through motor imagery (MI). In 2008, Choi and Cichocki[4] also designed a brain-controlled wheelchair based on MI, which can control the wheelchair to turn left, turn right, and go straight. Pires et al.[5] developed a brain-controlled wheelchair system based on P300 in 2008. The visual stimuli consisting of randomly augmented eight arrows were used to choose the direction in which the wheelchair was turned. Lee et al.[6] developed a brain-controlled mobile robot system using steady-state visual evoked potential (SSVEP) in 2012. The subjects can control the mobile robot to turn right and left and move forward by watching three visual stimuli displayed on the screen.

For a direct-brain-control robot, its computational complexity and cost are low. However, the kind of brain-controlled robots has some problems in practical application. For example, subjects who directly control the robot for a long time can feel tired easily, which can impair the control performance. In addition, safety is a big problem for direct-brain-control robots. Therefore, some researchers have proposed to introduce a certain level of autonomous robot control, forming a shared control strategy to overcome the weaknesses of direct brain-controlled robots. Iturrate et al.[7] developed a brain-controlled robotic wheelchair that first selects a destination through P300 BCI, and then the autonomous driving system is in charge of controlling the wheelchair to reach the selected destination. Deng et al.[8] developed the brain state evaluation network (BSE-NET), which can balance the control weight between human users and robot autonomy. Furthermore, Bi et al. first applied model predictive control with a BCI to develop a brain-control robot[9−11]. Liu et al. designed several control strategies to make sure the safety of brain-controlled robots[12, 13].

However, the existing studies on brain-controlled robots at the servo-control level focus on controlling a single robot. With the advancement of wireless communication technology and artificial intelligence technology, the cooperation between robots has become possible. Multi-robot systems can work together, perform complex tasks, and significantly improve work efficiency[14, 15]. The brain-controlled multi-robot system also has more significant advantages in assisting the disabled. For example, one person with disability can move by using a brain-controlled wheelchair (leader robot) and simultaneously carry daily necessities by follower robots. Such multi-robot systems can better assist patients in daily life.

Although there are some existing studies on brain-controlled multi-robots, they all use task-level control methods. Dai et al. designed different types of shared control multi-robot control systems, in which they used SSVEP BCIs to select the task of the system to improve the overall work efficiency[16, 17]. Kirchner et al.[18] applied a BCI to the level of task engagement, improving user support and the efficiency of interaction. Compared with the task-level system, the servo-level brain-controlled multi-robot framework can make the operators control the robots more freely.

Considering the potential application values of brain-controlled multi-robot systems at the servo-control level, in our previous conference paper[19], we introduced a BCI into a multi-robot system to develop a brain-controlled multi-robot system. However, the brain-controlled multi-robot system is simple and basic. Users cannot control the formation. In addition, the previous work only initially verified the feasibility of the multi-robot system in a simple simulation environment.

Thus, expanded from our previous work in Ref. [19], this paper explores how to control the direction, speed, and formation of a multi-robot system via electroencephalographic (EEG) signals and builds a complete brain-controlled multi-robot simulation and physical system. In particular, we propose a novel multi-robot predictive control framework (MRPCF), which can track users' control intentions and ensure the safety of multi-robots. The MRPCF consists of the leader controller, follower controller, and formation planner. The leader controller can track users' intentions (including left turn, right turn, acceleration, deceleration, start, and stop) and ensure the safe operation of the robot itself. The formation planner can track users' formation control intention, realize the safe transformation of multi-robot formation, output the optimized tracking target positions to the follower controller, and ensure no collision between follower robots. The follower controller can track the target positions and ensure the safety of the follower robots.

The new contributions of this paper are as follows:

(1) It is the first to investigate brain-controlled multi-robot systems' integrated lateral, longitudinal, and formation control.

(2) It proposes a novel multi-robot predictive control framework (MRPCF) for brain-controlled multi-robot systems at the servo-control level, which can track users' control intentions (including direction, speed, and formation intentions) while ensuring the safety of multi-robot systems.

(3) It builds a whole brain-controlled multi-robot physical system for the first time and validates the performance of the proposed system by human-in-the-loop actual experiments.

The structure of this paper is as follows. Section 2 presents the structure of the proposed brain-controlled multi-robot system. The proposed multi-robot predictive control framework is presented in Section 3. In Section 4, the human-in-the-loop brain-controlled multi-robot experiment is shown. The experimental results and discussion are given in Section 5. Conclusion and future work are described in Section 6.

2 Brain-Controlled Multi-Robot System

2.1 System structure

The structure diagram of a brain-controlled multi-robot system is shown in Fig. 1 and composed of a user, a BCI, a stimulus interface, an interface model, a leader robot, several follower robots, and the proposed MRPCF. The formation strategy of the system is based on the leader-follower model. In detail, in the multi-robot framework, one robot acts as the leader, and other robots maintain the relationship in direction and distance as followers and leaders.

This system can effectively improve the safety of users when using BCI to control the robot system. First, the user observes the environment and the state of the robot to make decisions and uses BCI to convey commands. Next, the interface model will quantify the control commands from human and input them to MRPCF. The MRPCF consists of a leader controller, follower controller, and formation planner. The leader controller will confirm if the system is safe with the information of the sensors and the robot itself. When safe, the controller will track the control intention of the user, otherwise, the controller will modify its control command output to ensure the system operation security. The formation planner can track users' formation control intention, realize the safe transformation of multi-robot formation, output the tracking target positions to the follower robots, and ensure no collision between follower robots. The follower controller ensures the follower robots travel safely and maintain formation.

2.2 Stimulus interface

In this part, the development of the multi-robot system adopts the BCI based on SSVEP. The BCI based on SSVEP has the superiority of fast command generation, high signal-to-noise ratio (SNR), and less training amount[20, 21]. The stimulus interface was designed with seven command labels and displayed them on the augmented reality (AR) glasses, as shown in Fig. 2. The flashing frequencies of command icons were preset to 13.00, 9.00, 10.00, 12.00, 11.00, 8.50, and 14.00 Hz, which represent speeding up (SU), slowing down (SD), turning left (TL), turning right (TR), maintaining speed (MS), formation reduction (FR), and formation enlargement (FE), respectively.

2.3 SSVEP-based BCI

The BCI based on SSVEP interprets users' EEG signals into commands for controlling multi-robots every 0.5 s. Let $I_C \in \{1,2,3,4,5,6,7\}$ represent the intentional commands decoded from users' EEG signals, where 1 stands for SU, 2 for FR, 3 for TL, 4 for MS, 5 for TR, 6 for SD, and 7 for FE, respectively.

EEG signals were acquired from eight standard channels (i.e., POz, PO3, PO4, PO5, PO6, Oz, O1, and O2) of an international 10-20 system by using a wireless EEG amplifier (NeuSen. W64, Neuracle,

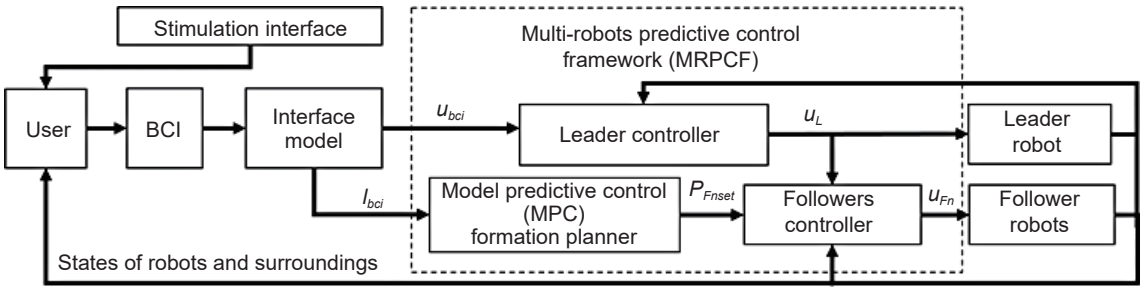

Fig. 1 Architecture of the proposed brain-controlled multi-robot system.

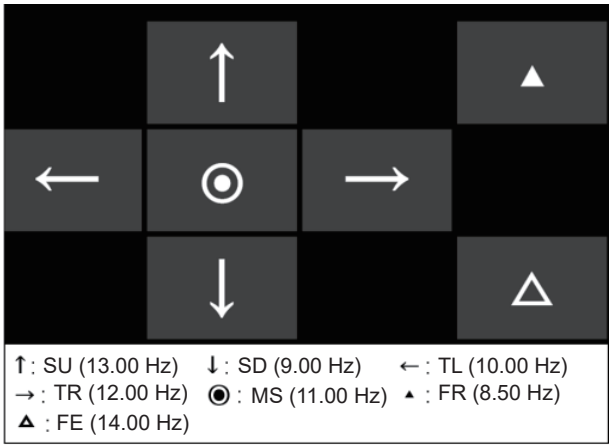

Fig. 2 Stimulus interface of BCI based on SSVEP.

China) with Ag/AgCl electrodes. The ground channel was positioned on AFz, and the reference channel was positioned on CPz. All of the electrodes' impedances were calibrated to keep lower than 10 kΩ. The EEG signals were magnified and digitalized at a sampling rate of 1 kHz. In addition, a filter bank canonical correlation analysis (CCA) was employed as a recognition model. More details about the algorithm of the BCI based on SSVEP can be found in Ref. [22].

2.4 Interface model

Since the output of SSVEP-based BCI is qualitative, the control command is quantified as

$$\begin{bmatrix} \omega_{bci}^{(k)} \\ v_{bci}^{(k)} \\ l_{bci}^{(k)} \end{bmatrix} = \begin{cases} \begin{bmatrix} \omega_{bci}^{(k-1)} & \min\left\{v_{bci}^{(k-1)}+\Delta v, v_{\max}\right\} & l_{bci}^{(k-1)} \end{bmatrix}^{\mathrm{T}}, \text{if } I_C^{(k)}=1; \\ \begin{bmatrix} \omega_{bci}^{(k-1)} & \max\left\{v_{bci}^{(k-1)}-\Delta v, v_{\min}\right\} & l_{bci}^{(k-1)} \end{bmatrix}^{\mathrm{T}}, \text{if } I_C^{(k)}=2; \\ \begin{bmatrix} \min\left\{\omega_{bci}^{(k-1)}+\Delta\omega, \omega_{\max}\right\} & v_{bci}^{(k-1)} & l_{bci}^{(k-1)} \end{bmatrix}^{\mathrm{T}}, \text{if } I_C^{(k)}=3; \\ \begin{bmatrix} \max\left\{\omega_{bci}^{(k-1)}-\Delta\omega, \omega_{\min}\right\} & v_{bci}^{(k-1)} & l_{bci}^{(k-1)} \end{bmatrix}^{\mathrm{T}}, \text{if } I_C^{(k)}=4; \\ \begin{bmatrix} \omega_{bci}^{(k-1)} & v_{bci}^{(k-1)} & l_{bci}^{(k-1)} \end{bmatrix}^{\mathrm{T}}, \text{if } I_C^{(k)}=5; \\ \begin{bmatrix} \omega_{bci}^{(k-1)} & v_{bci}^{(k-1)} & \min\left\{l_{bci}^{(k-1)}+\Delta l, l_{\max}\right\} \end{bmatrix}^{\mathrm{T}}, \text{if } I_C^{(k)}=6; \\ \begin{bmatrix} \omega_{bci}^{(k-1)} & v_{bci}^{(k-1)} & \max\left\{l_{bci}^{(k-1)}-\Delta l, l_{\min}\right\} \end{bmatrix}^{\mathrm{T}}, \text{if } I_C^{(k)}=7 \end{cases} \tag{1}$$

where $\omega_{bci}^{(k)}$, $v_{bci}^{(k)}$, and $l_{bci}^{(k)}$ represent the linear velocity, angular velocity, and commands of formation control at time k, respectively. $I_C^{(k)}$ is the output of the SSVEP-based BCI at time k. $v_{\max}$, $v_{\min}$, and Δv are the maximum, minimum, and increment of the linear velocity, respectively. $\omega_{\min}$ and $\omega_{\max}$ are the restricts of the robot angular velocity, and $\Delta\omega$ represents the angular velocity increment. $l_{\min}$ and $l_{\max}$ are the limits of the formation control, and Δl represents the formation control increment. Initially, the values of Δv, $v_{\min}$, and $v_{\max}$ were set to be 0.01, 0, and 0.04 m/s, respectively. The values of $\Delta\omega$, $\omega_{\min}$, and $\omega_{\max}$ were set to be 0.1, −0.2, and 0.2 rad/s, respectively. Δl, $l_{\min}$, and $l_{\max}$ were taken to be 0.10, 0.70, and 1.20 m, respectively.

2.5 Multi-robot model

In this article, the 2-wheel differential robot model is used in the experiment. The robot has two driving wheels and an auxiliary wheel (universal wheel). Independent direct current (DC) reduction motors drive both driving wheels. The different rotation speeds of the wheels can realize the forward, backward, and steering movements of the mobile robot. At the same time, we assume that there are no unexpected situations such as slipping and jumping when the robot moves in the plane, which means that there is a pure scrolling contact between the wheels and the ground[23].

We define the robot's state as $\boldsymbol{X}=\begin{bmatrix} x & y & \theta \end{bmatrix}^{\mathrm{T}}$ and control input as $\boldsymbol{u}=\begin{bmatrix} v & \omega \end{bmatrix}^{\mathrm{T}}$. Thus, in terms of the formation, the state of the leader robot is expressed as $\boldsymbol{X}_L=\begin{bmatrix} x_L & y_L & \theta_L \end{bmatrix}^{\mathrm{T}}$ and the input is $\boldsymbol{u}_L=\begin{bmatrix} v_L & \omega_L \end{bmatrix}^{\mathrm{T}}$. The state of the n-th follower robot is $\boldsymbol{X}_{Fn}=\begin{bmatrix} x_{Fn} & y_{Fn} & \theta_{Fn} \end{bmatrix}^{\mathrm{T}}$ and the robot's control input is $\boldsymbol{u}_{F_n}=\begin{bmatrix} v_{Fn} & \omega_{Fn} \end{bmatrix}^{\mathrm{T}}$, where x and y represent the robot's position, and θ is the orientation of the robot in the world coordinate system. v is the robot linear velocity, and ω is the robot angular velocity. The relationship between $\boldsymbol{X}$ and $\boldsymbol{u}$ is as follows:

$$\dot{\boldsymbol{X}}=\begin{bmatrix} \cos\theta & 0 \\ \sin\theta & 0 \\ 0 & 1 \end{bmatrix}\boldsymbol{u} \tag{2}$$

The leader-follower algorithm and the $l-\varphi$ formation control method are used for the multiple robot formation strategy. The positional relationship between the leader robot and the n-th follower robot is shown in Fig. 3. The formation control strategy is used to keep the distance and relative rotation orientation between the follower and leader robots[24]. As a result, regarding the n-th follower robot, the state parameters relative to the leading robot can be expressed as $\boldsymbol{E}_{Fnset}=\begin{bmatrix} l_{Fnset} & \varphi_{Fnset} \end{bmatrix}^{\mathrm{T}}$. And the tracking target positions of

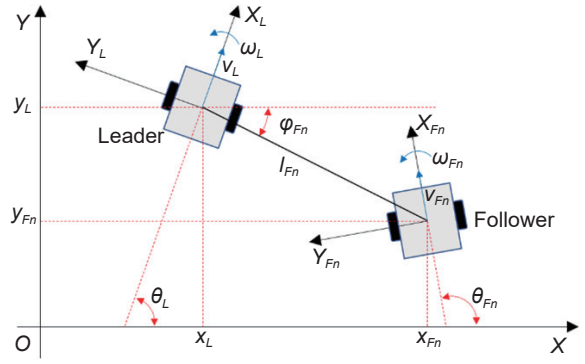

Fig. 3 Positional relationship between the leader robot and the follower robot.

the n-th follower robot are expressed as $\boldsymbol{P}_{Fnset} = \begin{bmatrix} x_{Fnset} & y_{Fnset} \end{bmatrix}^{\mathrm{T}}$, so the following relationship can be obtained

$$\begin{cases} x_{Fnset} = x_L + l_{Fnset}\cos\varphi_{Fnset}, \\ y_{Fnset} = y_L + l_{Fnset}\sin\varphi_{Fnset} \end{cases} \tag{3}$$

2.6 Multi-robot predictive control framework

The proposed MRPCF can track users' intentions and keep the multi-robots in safe. The MRPCF consists of the leader controller, follower controller, and formation planner. The leader controller optimizes the command output of the interface model according to the robot state and constraints, so as to ensure the robot in safe during operation. Similarly, the follower controller ensures that the follower robot runs safely. Finally, the formation planner solves the ideal target positions of the robots in the light of users' output command, and controls the formation change of the multi-robot system.

3 MRPCF Design

In this section, we introduce the MRPCF in detail. The framework consists of the leader controller, follower controller, and formation planner.

3.1 Leader controller

The leader controller allows the leader robot to track user control intentions (such as speeding up, slowing down, turning left, and turning right) when in safe. Assuming that users' brain controlled command input to the leader controller is $\boldsymbol{u}_{bci} = \begin{bmatrix} v_{bci} & \omega_{bci} \end{bmatrix}^{\mathrm{T}}$, the command $\boldsymbol{u}_L = \begin{bmatrix} v_L & \omega_L \end{bmatrix}^{\mathrm{T}}$ output by the controller is the input to the leader robot, the distance between the leader and the obstacle is d_L, and the safety distance is $D_{L\mathrm{safe}}$, we can define the objective and safety constraint of the leader controller based on MPC as follows:

$$\lim_{x\to\infty}(\boldsymbol{u}_L - \boldsymbol{u}_{bci}) = \boldsymbol{0} \tag{4}$$

$$d_L - D_{L\mathrm{safe}} \geqslant 0 \tag{5}$$

The whole formulation of the leader controller based on MPC can be designed as

$$\min \alpha\left(\boldsymbol{u}_L^{(k)} - \boldsymbol{u}_{bci}^{(k)}\right)^2 + \sum_{i=0}^{H_C-1}\left\|\boldsymbol{u}_L^{(k+i)} - \boldsymbol{u}_L^{(k+i-1)}\right\|_{\boldsymbol{Q}_L}^2 \tag{6}$$

s.t.

$$\begin{aligned} x_L^{(k+i+1)} &= x_L^{(k+i)} + v_L^{(k+i)} T_s \cos\theta_L^{(k+i)}, \\ y_L^{(k+i+1)} &= y_L^{(k+i)} + v_L^{(k+i)} T_s \sin\theta_L^{(k+i)}, \\ \theta_L^{(k+i+1)} &= \theta_L^{(k+i)} + \omega_L^{(k+i)} T_s, \quad i = 0,1,\ldots,H_P-1 \end{aligned} \tag{7}$$

$$D_{L\mathrm{safe}} - d_L^{(k+i+1)}\left(d_{obs}, \delta_{obs}, \boldsymbol{u}_L^{(k)}, \ldots, \boldsymbol{u}_L^{(k+i)}\right) \leqslant 0, \quad i = 0,1,\ldots,H_P-1 \tag{8}$$

$$\boldsymbol{u}_{L_{\min}} < \boldsymbol{u}_L^{(k+i)} < \boldsymbol{u}_{L_{\max}}, \quad i = 0,1,\ldots,H_C-1 \tag{9}$$

$$\Delta\boldsymbol{u}_L^{(k+i)} = \boldsymbol{u}_L^{(k+i)} - \boldsymbol{u}_L^{(k+i-1)}, \quad i = 0,1,\ldots,H_C-1 \tag{10}$$

$$\Delta\boldsymbol{u}_{L_{\min}} < \Delta\boldsymbol{u}_L^{(k+i)} < \Delta\boldsymbol{u}_{L_{\max}}, \quad i = 0,1,\ldots,H_C-1 \tag{11}$$

$$\Delta\boldsymbol{u}_L^{(k+i)} = 0, \quad i = H_C, H_C+1,\ldots,H_P-1 \tag{12}$$

where k is the current moment, H_P and H_C are the prediction and control horizons, respectively. T_s is the sampling period. α is the weighting factor to penalize control actions, and $\boldsymbol{Q}_L \in \mathbb{R}^{1\times H_C}$ is the weighting matrix that controls the change rate of the output.

The cost function (6) of the leader controller is able to make sure that the leader robot follows users' intentions, in which the first part punishes the performance of tracking, and the second part punishes smoothness of the control. Constraint (7) is the robot's prediction equation, which can predict the future status of the leader robot. Constraint (8) is designed to make sure the leader is in safe, where d_{obs} and δ_{obs} are the distance and angle of the nearest obstacle perceived by the radar, respectively. Constraints (9)−(11) are physical constraints. In addition, we set $H_C < H_P$ and presume the control signal to be constant for all $H_C \leqslant k \leqslant H_P$ to reduce the computation and complexity. Note that $\boldsymbol{u}_L^{(k-1)}$ denotes the output of controller in the former cycle.

3.2 Formation planner

For the $l-\varphi$ formation control strategy, to reduce

users' workload to control the multi-robot formation, we required users to only control the l, and the φ was pre-set. For the formation planner, it can solve the tracking target positions $\boldsymbol{P}_{Fnset}$ of the n-th follower robot according to the formation command l_{bci} output by users. The input is users' formation control commands, and the output is the tracking target positions $\boldsymbol{P}_{Fnset}$ to keep the follower robots from making collision with each other and the leader robot. Its control objective and safety constraint are

$$\lim_{x\to\infty}(l_{Fnset}-l_{bci})=0 \tag{13}$$

$$d_{\text{Formation}}-D_{\text{Formation\_safe}}\geqslant 0 \tag{14}$$

where $D_{\text{Formation\_safe}}$ is the safe distance between robots, and $d_{\text{Formation}}$ is the minimum distance between the current follower and other robots.

The whole formulation of the formation planner based on MPC is designed as

$$\min\gamma\left(l_{Fnset}^{(k)}-l_{bci}^{(k)}\right)^2+\sum_{i=0}^{H_C-1}\left\|l_{Fnset}^{(k+i)}-l_{Fnset}^{(k+i-1)}\right\|_{\boldsymbol{Q}_P}^2 \tag{15}$$

s.t.

$$x_{Fnset}^{(k+i)}=x_L^{(k)}+l_{Fnset}^{(k+i)}\cos\varphi_{Fnset},\quad i=0,1,\ldots,H_C-1 \tag{16}$$

$$y_{Fnset}^{(k+i)}=y_L^{(k)}+l_{Fnset}^{(k+i)}\sin\varphi_{Fnset},\quad i=0,1,\ldots,H_C-1 \tag{17}$$

$$\Delta x_{Fnset}^{(k+i)}=x_{Fnset}^{k+i}-x_{Fnset}^{k+i-1},\quad i=0,1,\ldots,H_C-1 \tag{18}$$

$$\Delta y_{Fnset}^{(k+i)}=y_{Fnset}^{k+i}-y_{Fnset}^{k+i-1},\quad i=0,1,\ldots,H_C-1 \tag{19}$$

$$\Delta x_{\min}<\Delta x_{Fnset}^{(k+i)}<\Delta x_{\max},\quad i=0,1,\ldots,H_C-1 \tag{20}$$

$$\Delta y_{\min}<\Delta y_{Fnset}^{(k+i)}<\Delta y_{\max},\quad i=0,1,\ldots,H_C-1 \tag{21}$$

$$l_{Fn_{\min}}<l_{Fnset}^{(k+i)}<l_{Fn_{\max}},\quad i=0,1,\ldots,H_C-1 \tag{22}$$

$$D_{\text{Formation\_safe}}-d_{\text{Formation}}^{(k+i+1)}\leqslant 0,\quad i=0,1,\ldots,H_P-1 \tag{23}$$

where γ is the weight factor to penalize the formation control actions, and $\boldsymbol{Q}_P\in\mathbb{R}^{1\times H_C}$ is the weight matrix of the control output's rate of change. The above optimization problem can ensure that the output formation is safe. Constraints (16)−(22) are physical constraints. In Constraints (18) and (19), Δx and Δy are the change rates of tracking target positions. Constraints (20) and (21) are used to limit the tracking of target position changes. Constraint (23) is a safety constraint to ensure that the robots do not collide with each other.

3.3 Follower controller

The follower controller enables each follower robot to track its target positions $\boldsymbol{P}_{Fnset}$ planned by the formation planner in safe. Therefore, the major control objectives are defined as

$$\lim_{x\to\infty}e_n=0 \tag{24}$$

$$\lim_{x\to\infty}(\boldsymbol{u}_{Fn}-\boldsymbol{u}_L)=\boldsymbol{0} \tag{25}$$

where e_n is the passional error between the current moment location of the n-th follower robot and the robot's target location. The control objective of Eq. (25) is to keep the speed of the n-th follower robot consistent with which of the leader to maintain the formation when the n-th follower robot is near the target point.

The safety constraint can be written as

$$d_F-D_{F\text{safe}}\geqslant 0 \tag{26}$$

where $D_{F\text{safe}}$ represents the robot's safe distance, and d_F is the distance from the robot to barriers.

The whole formulation of the follower controller for the n-th follower robot based on MPC is designed as

$$\begin{aligned}\min&\sum_{i=0}^{N_P-1}\beta\left(e_n^{(k+i+1)}\right)^2+\lambda\left(\boldsymbol{u}_{Fn}^{(k)}-\boldsymbol{u}_L^{(k)}\right)^2+\\&\sum_{i=0}^{H_C-1}\left\|\boldsymbol{u}_{Fn}^{(k+i)}-\boldsymbol{u}_{Fn}^{(k+i-1)}\right\|_{\boldsymbol{Q}_F}^2\end{aligned} \tag{27}$$

s.t.

$$\begin{aligned}x_{Fn}^{(k+i+1)}&=x_{Fn}^{(k+i)}+v_{Fn}^{(k+i)}T_s\cos\theta_{Fn}^{(k+i)},\\y_{Fn}^{(k+i+1)}&=y_{Fn}^{(k+i)}+v_{Fn}^{(k+i)}T_s\sin\theta_{Fn}^{(k+i)},\\\theta_{Fn}^{(k+i+1)}&=\theta_{Fn}^{(k+i)}+\omega_{Fn}^{(k+i)}T_s,\quad i=0,1,\ldots,H_P-1\end{aligned} \tag{28}$$

$$e_n^{(k+i+1)}=\sqrt{\left(x_{Fn}^{(k+i+1)}-x_{Fnset}^{(k+i+1)}\right)^2+\left(y_{Fn}^{(k+i+1)}-y_{Fnset}^{(k+i+1)}\right)^2},\quad i=0,1,\ldots,H_P-1 \tag{29}$$

$$D_{F\text{safe}}-d_F^{(k+i+1)}\leqslant 0,\quad i=0,1,\ldots,H_P-1 \tag{30}$$

$$\boldsymbol{u}_{F_{\min}}<\boldsymbol{u}_{Fn}^{(k+i)}<\boldsymbol{u}_{F_{\max}},\quad i=0,1,\ldots,H_C-1 \tag{31}$$

$$\Delta\boldsymbol{u}_F^{(k+i)}=\boldsymbol{u}_{Fn}^{(k+i)}-\boldsymbol{u}_{Fn}^{(k+i-1)},\quad i=0,1,\ldots,H_C-1 \tag{32}$$

$$\Delta\boldsymbol{u}_{F_{\min}}<\Delta\boldsymbol{u}_{F_n}^{(k+i)}<\Delta\boldsymbol{u}_{F_{\max}},\quad i=0,1,\ldots,H_C-1 \tag{33}$$

In Formula (27), β is the weight factor of penalizing the tracking error of the follower robot, λ is the weighting factor to penalize the control actions, and

$\boldsymbol{Q}_F \in \mathbb{R}^{1\times H_C}$ is the weighting matrix of the change rate of control signals. The cost function (27) is designed to make sure that the n-th follower robot follows the target point $\boldsymbol{P}_{Fnset}$. Equation (28) is the prediction equation, which can be used to predict the future positions of the n-th follower robot. Formula (30) is a safety constraint, which can stipulate the safety distance between the n-th follower robot and the obstacle to ensure the safe operation of the system.

4 Brain-Controlled Multi-Robot Experiment

To verify and evaluate the performance of the proposed MRPCF, we set up a whole brain-controlled multi-robot physical system and physical experimental scene and conducted a human-in-the-loop brain-controlled multi-robot experiment.

4.1 Participant

Four subjects (aged 20−25 years old) participated in this experiment. All subjects had no history of brain-related diseases and had normal or corrected-to-normal vision. Each subject had enough sleep and a good mental state before the experiment. The study complied with the principles of the 2013 Declaration of Helsinki and was approved by the local research ethics committee. In addition, each subject signed the experimental informed form.

Before starting the experiment, we required the subjects to be familiar with the experimental protocol and procedure. As shown in Fig. 4, the subject sat on a comfortable chair during the experiment and wore an EEG collection cap and AR glasses (LINGXI-AR Inc., China).

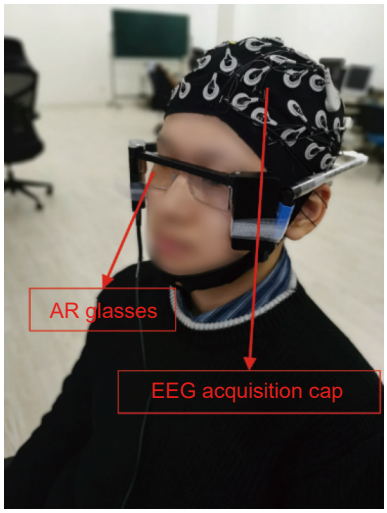

Fig. 4 Experimental setup for subjects.

4.2 Experimental platform

Figure 5 shows the human-in-the-loop multi-robot experimental scene. We set two destinations (Positions A and B) in the scene. We also set up two types of obstacles, namely obstacle-O_1 and obstacle-O_2. Obstacle-O_1 can be detected by the radar of the robots, whereas the robots cannot perceive obstacle-O_2. A narrow passage was formed between the two obstacle-O_2s, and multi-robots were required to pass through this passage during the navigation control. The initial positions of the multi-robots were in a regular triangle, as shown in Fig. 5, in which the leader robot was located on the tip, and the two follower robots were located on both sides. The model of the leader robot was Turtlebot3 Waffle-Pi, and the model of the follower robots was Turtlebot3 Burger. Turtlebot3 robot is a small, low-cost, fully programmable, robot operating system (ROS) based two-wheeled differential mobile robot. Every robot was equipped with a radar for perceiving environmental information (HLS-LFCD2). In addition, the encoder arranged on the motor can be used to estimate the state of the robots.

The stimulation interface was developed by Matlab/Psychophysics Toolbox, and the SSVEP-based BCI system was developed in M code. The matlab-robot operating system (ROS) node sent the control signals quantized by the interface model to the ROS system. The proposed control framework MRPCF was built based on the ROS system development, which received the quantized control signals and sent them to each robot.

4.3 Parameter setup

Parameters of the MRPCF consisted of the leader

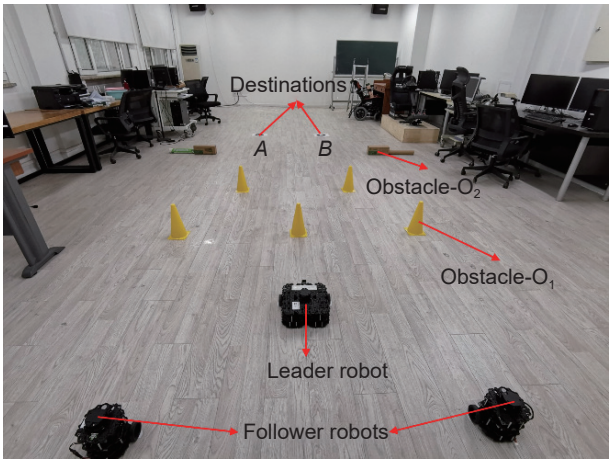

Fig. 5 Human-in-the-loop multi-robot experimental setup.

controller, follower controller, and formation planner parameters. We used the trial-and-error method to determine the weight factors, prediction and control horizons, and safe distances. Because the models of the leader robot and follower robots were different, we set different safe distances. Considering that the leader control can only obtain the reference input of the subjects at the current moment, we design the control horizons H_C of the leader controller to be 1. The parameters of the proposed controller were set, as shown in Table 1.

4.4 Experimental procedure and evaluation metrics

This experiment was divided into two stages: (1) the offline testing stage; (2) the online navigation stage.

Table 1 Parameters of MRPCF.

Type	Symbol	Value
Leader controller	T_s	0.5 s
	H_C	1
	H_P	4
	α	2
	$\boldsymbol{Q}_L$	$[1 \quad 1 \quad 1]^{\mathrm{T}}$
	$\boldsymbol{u}_{L\min}$	[0 m/s; −0.2 rad/s]
	$\boldsymbol{u}_{L\max}$	[0.04 m/s; 0.2 rad/s]
	$\Delta\boldsymbol{u}_{L\min}$	[−0.02 m/s; −0.1 rad/s]
	$\Delta\boldsymbol{u}_{L\max}$	[0.02 m/s; 0.1 rad/s]
	$D_{L\text{safe}}$	0.25 m
Formation planner	T_s	0.5 s
	H_C	1
	H_P	4
	γ	2
	$\boldsymbol{Q}_P$	$[1 \quad 1 \quad 1]^{\mathrm{T}}$
	$\Delta x_{\min}$	−0.02 m
	$\Delta x_{\max}$	0.02 m
	$\Delta y_{\min}$	−0.02 m
	$\Delta y_{\max}$	0.02 m
	$D_{\text{Fomation\_safe}}$	0.15 m
Follower controller	T_s	0.25 s
	H_C	20
	H_P	20
	β	5
	λ	1
	$\boldsymbol{Q}_F$	$[1 \quad 1 \quad \cdots \quad 1]^{\mathrm{T}}$
	$\boldsymbol{u}_{F_{\min}}$	[0 m/s; −0.4 rad/s]
	$\boldsymbol{u}_{F_{\max}}$	[0.06 m/s; 0.4 rad/s]
	$\Delta\boldsymbol{u}_{F_{\min}}$	[−0.02 m/s; −0.1 rad/s]
	$\Delta\boldsymbol{u}_{F_{\max}}$	[0.02 m/s; 0.1 rad/s]
	$D_{F\text{safe}}$	0.04 m

The purpose of the offline testing was to calibrate and evaluate the SSVEP-based BCI system. During this stage, the subjects were asked to concentrate on each command stimulus for 1 min, and the response time of the BCI was 0.5 s. Therefore, for each command, there were a total of 120 samples. Using the FBCCA algorithm in Ref. [22], we obtained the recognition results of all samples of each command and computed the recognition accuracy of each command.

When the average accuracy of all commands was larger than 70%, the subjects were qualified for the online navigation task. The navigation task was to control the multi-robots from the initial position to the designated target position (*A* or *B*) in a limited time while avoiding obstacles. If the leader robot reached within 0.2 m around the target position within the timeout limit, we considered that the task was completed successfully. The experimental timeout condition is set to three times the time it takes for the leader robot to reach the destination in a straight line at the highest speed.

In this stage, we set up three tasks: (1) the brain-controlled online navigation task, (2) the manual-control online navigation task simulating the condition of the BCI with an accuracy of 100%, and (3) the formation transformation task. In task (1), we made the comparison between the brain-controlled navigation task with and without the proposed MRPCF. Without MRPCF, the commands output by the SSVEP-based BCI system directly control the robot cluster, and subjects rely on the brain-computer interface to output commands to ensure the system runs safely and reaches the target position. In this task, subjects were required to reach target locations *A* and *B* twice under each control condition. Figure 6 shows a subject performing a brain-controlled online navigation task. In task (2), the only difference from task (1) was that the control signal was output by users pressing the keyboard by hands rather than through the BCI. We set the same commands on the keyboard as in the stimulation interface, and keyboard commands were output every 0.5 s.

In addition, for the above two tasks, the trials of different control modes (i.e., with and without the MRPCF) were counterbalanced in random order. In the above two tasks, subjects did not need to change the formation of robots. Therefore, for the tasks assisted by the MRPCF, we deactivated the formation

Fig. 6 Brain-controlled online navigation scene.

transformation commands. To reduce unwanted effects, subjects will rest for five minutes after each control trial.

Finally, to verify the proposed controller's performance more intuitively, we set up task (3). In this task, we need subjects to control the robot formation through BCI to change formation and pass through the obstacle area to reach the designated place. The subjects were required to control the multi-robot to arrive at each destination twice in different formation transformations (zooming in or out).

To evaluate the performance of the online navigation task, we used these metrics: (1) Task completion rate (CR), defined as the proportion of the tasks completed in the total; (2) Number of collisions (NC), defined as the number of times that robots collided with obstacles, (3) Task completion time (CT), defined as the time taken by the multi-robot system from the initial position to the destination, (4) Driving distance (DD), defined as the distance travelled by the leader robot in each control cycle; and (5) Average speed (AS), the average speed of the leader robot. Furthermore, we required all subjects to complete a questionnaire survey (QS) used for subjective evaluation of the system after the first task was completed.

5 Experimental Results and Discussion

5.1 Performance of the SSVEP-based BCI

Table 2 shows the accuracy of SSVEP BCI across all subjects obtained in the offline test stage. It was found that the highest accuracy was 100.00% (SU command for Subject S1), and the lowest accuracy was 61.21% (FR command for Subject S4). In addition, compared with other subjects, the average accuracy of Subject S4 was relatively low. The results show that the average BCI accuracy rate of all participants is above 70%, which meets the basic conditions for the online navigation stage task.

5.2 Brain-controlled online navigation performance

Table 3 shows the performance comparison of brain-controlled multi-robot navigation tasks with and without the MRPCF. Note that, for the metrics DD, AS, and CT, we only counted the trials where the tasks were completed successfully, whereas, for NC, we counted all trials. From Table 3, we found that with the MRPCF, the average CR reached (100.00±0.00)%. In contrast, without the MRPCF, the average CR was (37.50±14.43)%. With the MRPCF, there was no collision for each subject (i.e., all NC were 0.00). In comparison, without the MRPCF, the average NC was 0.94±0.24.

Compared with the direct control (i.e., without the MRPCF), the MRPCF shortened the DD and increased AS by 9.19% and 12.97%, respectively. Furthermore, there was a difference in CT with and without the MRPCF (165.28±222.88 versus 205.39±34.16), showing that by using the proposed MRPCF, CT was improved by 19.53%. These experimental results showed that the proposed MRPCF could make up for the shortcomings of the direct control, improve the performance of the brain-controlled multi-robot system, and ensure the safety of the brain-controlled multi-robot system. The reason for these findings was likely that the MRPCF had safety constraints and the functions of assisting obstacle avoidance and keeping

Table 2 Performance of the SSVEP BCI.

Subject	Accuracy of SSVEP BCI (%)							
	SU	TL	MS	TR	SD	FR	FE	Mean ± standard deviation
S1	100.00	92.71	92.73	99.64	99.66	93.73	95.01	96.21±3.16
S2	94.10	94.91	97.32	98.22	79.20	96.61	93.97	93.47±6.01
S3	95.41	94.14	98.32	98.32	98.00	98.55	94.86	96.80±1.77
S4	72.57	75.00	96.55	82.46	73.45	61.21	76.52	76.82±9.98

Table 3 Performance comparison of brain-controlled navigation tasks with and without MRPCF. Note that CR is task completion rate, NC is number of collisions, CT is task completion time, DD is driving distance, and AS is average speed.

Modality	Subject	CR (%)	Mean ± STD of CR (%)	NC	Mean ± STD of NC (%)	CT (s)	Mean ± STD of CT (%)	DD (m)	Mean ± STD of DD (%)	AS (m/s)	Mean ± STD of AS (%)
With MRPCF	S1	100.00	100.00± 0.00	0.00± 0.00	0.00± 0.00	148.75± 7.79	165.28± 222.88	5.64± 0.29	5.83± 0.20	0.0379± 0.000 25	0.0357± 0.003 40
	S2	100.00		0.00± 0.00		148.35± 7.19		5.68± 0.25		0.0383± 0.000 84	
	S3	100.00		0.00± 0.00		166.98± 2.97		5.98± 0.37		0.0356± 0.002 07	
	S4	100.00		0.00± 0.00		197.02± 23.19		6.03± 0.63		0.0309± 0.000 74	
Without MRPCF	S1	25.00	37.50± 14.43	0.75± 0.50	0.94± 0.24	163.00± 0.00	205.39± 34.16	5.88± 0.00	6.42± 0.49	0.0361± 0.000 00	0.0316± 0.003 25
	S2	25.00		0.75± 0.50		192.40± 0.00		6.15± 0.00		0.0317± 0.000 00	
	S3	50.00		1.00± 0.00		234.20± 10.78		6.92± 0.05		0.0292± 0.001 63	
	S4	50.00		1.25± 0.50		231.95± 6.43		6.74± 0.06		0.0292± 0.001 20	

Note: STD is the standard deviation.

formation.

Figure 7 shows the trajectories of navigation tasks with and without MRPCF, respectively. The orange areas *A* and *B* represent the destination of each mission, the yellow circles represent obstacles on the way of the mission, the black solid lines represent the trajectory of each robot (the path of the leader robot is the thick solid line), and the gray dash-line triangles indicate the position of the multi-robots at a certain moment, which can reflect the multi-robot formation. Furthermore, the triangles in Fig. 7 are screenshots of the formation with an interval of 10 s, and the vertices of the triangles are the positions of the robots. The density between the triangles can show the difference in the speed of the system.

From Fig. 7, it can be pointed out that the brain-controlled multi-robot system with the MRPCF can avoid obstacles while navigation. For the leader robot, when the brain control commands did not ensure the safety of the robot, the proposed MRPCF can output safe control commands. For follower robots, when obstacles threaten the safety of the robot, the proposed controller can change the formation of multi-robots to avoid obstacles. When the surroundings are safe, the MRPCF can ensure the tracking of the desired formation. In contrast, subjects without MRPCF require to specifically secure the system through BCI commands. Therefore, from Fig. 7b, we saw that the trajectory of multi-robots while contouring obstacle-O_1 was very tortuous. Also, the density of triangles shows that the system in Fig. 7b spends more time traversing the obstacle area. The main reason is that the subjects need to constantly change the direction of the robot formation to avoid collisions with obstacles.

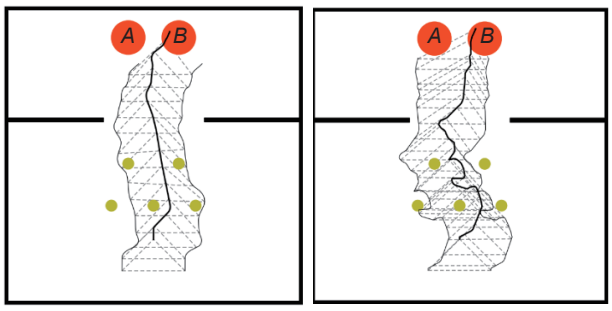

Fig. 7 Trajectories of multi-robot navigation tasks with and without MRPCF for a subject.

Figure 8 shows the linear velocity profiles of the leader robot with and without MRPCF for a subject. The red curve is the velocity profile of the leader robot with the MRPCF. The blue dotted line represents the velocity profile of the leader without the MRPCF. Time *a* and Time *b* represent the time points of reaching the destination under the MRPCF and direct control, respectively. From Fig. 8, we found that, compared to the direct control, the MRPCF made the leader robot run at a relatively higher linear velocity at most time, which indicated that our method improved the control ability of brain-controlled subjects. Combining the subjects' statements and trajectories, we can see that the high-frequency deceleration of the direct brain-controlled multi-robot system is to avoid

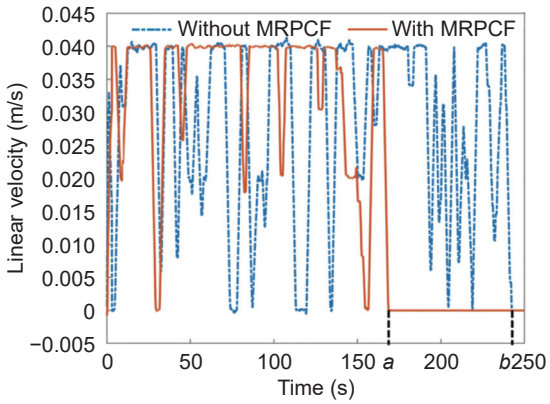

Fig. 8 Linear velocity profiles of the leader robot with and without MRPCF for a subject.

collisions between robots and obstacles to ensure the safety of the system.

Figure 9 shows the input and output linear and angular velocity profiles of the leader controller in the navigation stage for a subject, respectively. The input velocity is represented by a blue dotted line and the output velocity by a black curve. The input velocity commands were generated by the brain-controlled subjects, and the output velocity commands were generated by the leader controller. In the red circle, we can see that the input command was $\boldsymbol{u}_{bci} = \begin{bmatrix} 0.04 & 0.0 \end{bmatrix}^{\mathrm{T}}$, and the output command was corrected to be about $\boldsymbol{u}_L = \begin{bmatrix} 0.02 & -0.2 \end{bmatrix}^{\mathrm{T}}$. The reason for correcting the input velocity was that, as shown in Fig. 5, brain-controlled subjects first needed to issue a speeding-up command to start the multi-robot system. Since there was an obstacle-O_1 in right front of the leader robot, the leader robot has the possibility of colliding with obstacle-O_1. Thus, the leader controller reduced the linear velocity of the multi-robots and started to steer the multi-robots to avoid obstacle-O_1. Similarly, the same situation also occurred at about time 45 s. The leader controller actively slowed down the multi-robots to ensure safety. At other time, the input and output velocities were approximately identical. The reason for this may be that the safety of the leader robot was guaranteed, so the leader

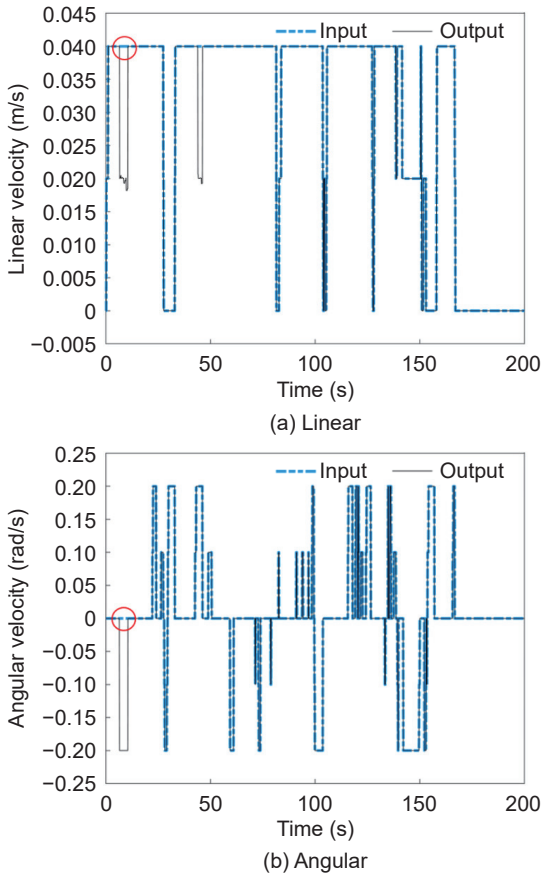

Fig. 9 Input and output linear and angular velocity profiles of the leader controller in the navigation stage for a subject.

controller tracked the commands output by subjects.

Furthermore, we found that, during the entire navigation process, to ensure safety, the controller took 6.2 s and 4.0 s to actively adjust the linear and angular velocities, accounting for 3.67% and 2.37% of the entire process, respectively. The results showed that the leader controller almost completely tracked the subject's intentions during the execution of the task, except for the necessary safety.

After the human-in-the-loop brain-controlled multi-robot experiment, we conducted a questionnaire survey for all subjects to evaluate two control methods. As shown in Table 4, the questionnaire consisted of three questions, and the answer to each question was on a

Table 4 Subjective questionnaire.

No.	Question	Score 1	Score 2	Score 3	Score 4	Score 5
Q1	Under this control mode, do you have the feeling of controlling the motion of multiple robots?	Not at all	Little	Some	A lot	Totally
Q2	Under this control mode, how much effort do you think it takes to control multiple robots?	A lot	Much	Some	A little	None
Q3	To what extent do you prefer to use this control mode?	Not at all	A little	Some	Much	A lot

scale of 1−5.

In Fig. 10, the subjective evaluation results are shown as a histogram. In the control feeling question (Q1), the subjects had more strong feelings in control of robots under the MRPCF than under the direct control (4.75±0.50 versus 3.00±0.82). In the control effort question (Q2), it was easier for the subjects to control multiple robots under the MRPCF than under the direct control (3.25±0.95 versus 1.75±0.50). Moreover, in the control preference (Q3), brain-controlled subjects preferred the proposed MRPCF to the direct control (4.25±0.50 versus 2.50±0.58).

5.3 Manual-control online navigation performance

All subjects completed the manual-control online navigation task, so the CR was 100%. Furthermore, multi-robots did not collide with any obstacles for all subjects, except Subject 3. For Subject 3, multi-robots collided with obstacles twice during the direct manual-control navigation. Although the direct manual-control navigation performance was pretty good, with the addition of the MRPCF, the safety of the multi-robots was guaranteed for all subjects. That is, there was no collision during the whole navigation for all subjects under the MRPCF.

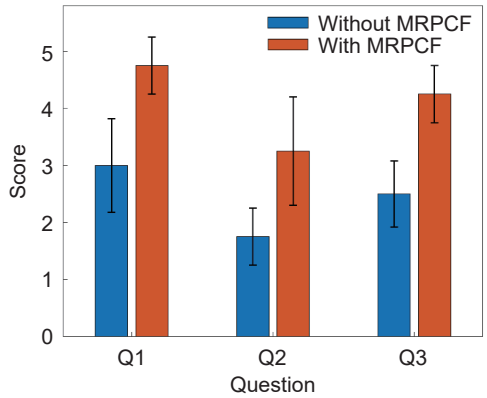

Fig. 10 Subjective questionnaire results.

Table 5 shows the performance comparison of manual-control multi-robot navigation tasks with and without MRPCF. By comparing the metrics, we found that, under the direct manual control, the average CT, DD, and AS of all subjects were 158.16±16.07 s, 5.72±0.28 m, and 0.0363±0.001 65 m/s, respectively. After introducing the proposed MRPCF, the average metrics CT, DD, and AS were 140.58±3.06 s, 5.37±0.12 m, and 0.0381±0.00012 m/s, respectively. That is, the MRPCF improved the three metrics by 11.11%, 6.12%, and 4.96%, respectively. Therefore, the proposed MRPCF can improve the system performance even for traditional control methods (manual control), demonstrating the effectiveness of MRPCF.

5.4 Formation transformation performance

We changed the task content, asking subjects to change the multi-robot formation and reach the designated destination under the MRPCF. Figure 11 shows trajectories of the formation of the multi-robot system. In Fig. 11a, the subject controlled the system to cross the obstacle area expanding the formation to reach destination *A*. Similarly, in Fig. 11b, the subject controlled the formation reducing the formation to reach destination *B*. The results showed that the subjects were able to complete the specified formation changes and reach the specified destination under the MRPCF.

In the entire moving process of the multi-robot system, the proposed MRPCF was able to perform the formation transformation and guarantee the safety of the multi-robot system. However, we found that after introducing the formation change command, the follower robots' movement trajectory was more tortuous. This phenomenon may be triggered by formation command errors caused by BCI accuracy.

Table 5 Performance of manual-control multi-robot navigation tasks with and without MRPCF. Note that CT is task completion time, DD is driving distance, and AS is average speed.

Modality	Subject	CT (s)	Mean of CT (%)	DD (m)	Mean of DD (%)	AS (m/s)	Mean of AS (%)
With MRPCF	S1	142.00±6.50	140.58±3.06	5.47±0.19	5.37±0.12	0.0382±0.000 56	0.0381±0.000 12
	S2	139.80±1.76		5.33±0.12		0.0380±0.000 51	
	S3	143.80±1.30		5.48±0.03		0.0380±0.000 55	
	S4	136.70±4.53		5.22±0.15		0.0382±0.000 23	
Without MRPCF	S1	144.00±1.66	158.16±16.07	5.49±0.09	5.72±0.28	0.0378±0.000 31	0.0363±0.001 65
	S2	152.90±22.26		5.63±0.27		0.0371±0.003 42	
	S3	181.25±27.05		6.12±0.45		0.0340±0.002 65	
	S4	154.48±4.18		5.64±0.11		0.0364±0.000 80	

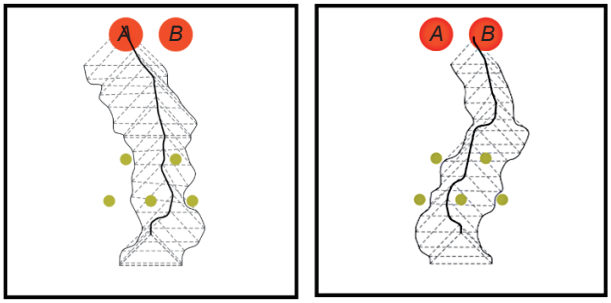

Fig. 11 Trajectories of multi-robot formation for a subject. (a) Result of the task where the subject was required to reach the target position *A* and the formation is enlarged. (b) Result of the task to go to the target position *B* and the formation is reduced.

6 Conclusion

This paper investigated the integrated lateral, longitudinal, and formation control of brain-controlled multi-robot systems by proposing a novel multi-robot predictive control framework (MRPCF), which can track users' control intentions and ensure the safety of multi-robots, and built an entire brain-controlled multi-robot system based on the proposed MRPCF for the first time. The proposed MRPCF consisted of the leader controller, follower controller, and formation planner. We validated the performance of the proposed system through human-in-the-loop actual experiments. The experimental results showed the effectiveness of the proposed method in tracking users' lateral, longitudinal, and formation control of brain-controlled multi-robot systems and maintaining the safety of brain-controlled multi-robot systems.

This work has value in moving the study of brain-controlled robots toward a new direction of brain-controlled multi-robots and provides some new insights into human-machine collaboration and integration. However, several challenges still need to be addressed, and they open future research opportunities along in this direction.

First, during the entire experiment with the MRPCF, the safety distance was fixed. In the next step, we should improve the safety distance for better robot performance, in which safety distance can change with different speeds.

Second, in our formation transformation task, the multi-robot formation was relatively simple. It was only limited to the enlargement and reduction of the formation. In the future, we should expand the function of formation to adapt to more complex scenarios. In addition, we need to improve the interface model to reduce the cases where the mind-controlled user falsely triggers the command by mistake.

Third, our experimental scene was still relatively simple, where only static obstacles existed. In the future, we should introduce dynamic obstacles to better validate the performance of the proposed method.

Our future work aims to address the issues mentioned above, including adjusting the safety distance, testing more formations, introducing dynamic obstacles, and improving the control method's performance by combining other intelligent technologies.

Acknowledgment

This work was supported by the National Natural Science Foundation of China (No. 51975052).

References

[1] M. A. Lebedev and M. A. L. Nicolelis, Brain-machine interfaces: Past, present and future, *Trends in Neurosciences*, vol. 29, no. 9, pp. 536–546, 2006.

[2] J. D. R. Millán, F. Renkens, J. Mouriño, and W. Gerstner, Noninvasive brain-actuated control of a mobile robot by human EEG, *IEEE Trans. Biomed. Eng.*, vol. 51, no. 6, pp. 1026–1033, 2004.

[3] K. Tanaka, K. Matsunaga, and H. O. Wang, Electroencephalogram-based control of an electric wheelchair, *IEEE Trans. Robot.*, vol. 21, no. 4, pp. 762–766, 2005.

[4] K. Choi and A. Cichocki, Control of a wheelchair by motor imagery in real time, in *Proc. 9th International Conference on Intelligent Data Engineering and Automated Learning*, Daejeon, Republic of Korea, 2008, pp. 330–337.

[5] G. Pires, M. Castelo-Branco, and U. Nunes, Visual P300-based BCI to steer a wheelchair: A Bayesian approach, in *Proc. 2008 30th Annu. Int. Conf. IEEE Eng. Med. Biol. Soc.*, Vancouver, Canada, 2008, pp. 658–661.

[6] P. L. Lee, H. C. Chang, T. Y. Hsieh, H. T. Deng, and C. W. Sun, A brain-wave-actuated small robot car using ensemble empirical mode decomposition-based approach, *IEEE Trans. Syst. Man, Cybern. Part A: Systems Humans*, vol. 42, no. 5, pp. 1053–1064, 2012.

[7] I. Iturrate, J. M. Antelis, A. Kübler, and J. Minguez, A noninvasive brain-actuated wheelchair based on a P300 neurophysiological protocol and automated navigation, *IEEE Trans. Robot.*, vol. 25, no. 3, pp. 614–627, 2009.

[8] X. Deng, Z. L. Yu, C. Lin, Z. Gu, and Y. Li, Self-adaptive shared control with brain state evaluation network for human-wheelchair cooperation, *J. Neural Eng.*, vol. 17, no. 4, p. 045005, 2020.

[9] L. Bi, M. Wang, Y. Lu, and F. A. Genetu, A shared controller for brain-controlled assistive vehicles, in *Proc. 2016 IEEE International Conference on Advanced Intelligent Mechatronics* (*AIM*), Banff, Canada, 2016, pp. 125–129.

[10] F. He, L. Bi, Y. Lu, H. Li, and L. Wang, Model predictive

control for a brain-controlled mobile robot, in *Proc. 2017 IEEE International Conference on Systems, Man, and Cybernetics* (*SMC*), Banff, Canada, 2017, pp. 3184–3188.
[11] H. Li, L. Bi, and J. Yi, Sliding-mode nonlinear predictive control of brain-controlled mobile robots, *IEEE Trans. Cybern.*, vol. 52, no. 6, pp. 5419–5431, 2020.
[12] R. Liu, K. Z. Xue, Y. X. Wang, and L. Yang, A fuzzy-based shared controller for brain-actuated simulated robotic system, in *Proc. 2011 Annu. Int. Conf. IEEE Eng. Med. Biol. Soc.* (*EMBS*), Boston, MA, USA, 2011, pp. 7384–7387.
[13] R. Liu, Y. X. Wang, and L. Zhang, An FDES-based shared control method for asynchronous brain-actuated robot, *IEEE Trans. Cybern.*, vol. 46, no. 6, pp. 1452–1462, 2016.
[14] Y. U. Cao, A. S. Fukunaga, and A. B. Kahng, Cooperative mobile robotics: Antecedents and directions, *Auton. Robots*, vol. 4, no. 1, pp. 7–27, 1997.
[15] T. Balch and R. C. Arkin, Behavior-based formation control for multirobot teams, *IEEE Trans. Robot. Autom.*, vol. 14, no. 6, pp. 926–939, 1998.
[16] W. Dai, Y. Liu, H. Lu, Z. Zheng, and Z. Zhou, A shared control framework for human-multirobot foraging with brain-computer interface, *IEEE Robotics and Automation Letters*, vol. 6, no. 4, pp. 6305–6312, 2021.
[17] W. Dai, Y. Liu, H. Lu, Z. Zhou, and Z. Zhen, Shared control based on a brain-computer interface for human-multirobot cooperation, *IEEE Robotics and Automation Letters*, vol. 6, no. 3, pp. 6123–6130, 2021.
[18] E. A. Kirchner, S. K. Kim, M. Tabie, H. Wohrle, M. Maurus, and F. Kirchner, An intelligent man-machine interface-multi-robot control adapted for task engagement based on single-trial detectability of P300, *Front Hum Neurosci*, vol. 10, p. 291, 2016.
[19] E. Li, L. Bi, and W. Chi, Brain-controlled leader-follower robot formation based on model predictive control, in *Proc. 2020 IEEE/ASME Int. Conf. Adv. Intell. Mechatronics* (*AIM*), Boston, MA, USA, 2020, pp. 290–295.
[20] M. Liu, K. Wang, X. Chen, J. Zhao, Y. Chen, H. Wang, J. Wang, and S. Xu, Indoor simulated training environment for brain-controlled wheelchair based on steady-state visual evoked potentials, *Front. Neurorobot.*, vol. 13, p. 101, 2019.
[21] L. Bi, X. A. Fan, K. Jie, T. Teng, H. Ding, and Y. Liu, Using a head-up display-based steady-state visually evoked potential brain-computer interface to control a simulated vehicle, *IEEE Trans. Intell. Transp. Syst.*, vol. 15, no. 3, pp. 959–966, 2014.
[22] X. Chen, Y. Wang, S. Gao, T. P. Jung, and X. Gao, Filter bank canonical correlation analysis for implementing a high-speed SSVEP-based brain-computer interface, *J. Neural Eng.*, vol. 12, no. 4, p. 046008, 2015.
[23] G. Campion, G. Bastin, and B. Dandréa-Novel, Structural properties and classification of kinematic and dynamic models of wheeled mobile robots, *IEEE Trans. Robot. Autom.*, vol. 12, no. 1, pp. 47–62, 1996.
[24] A. K. Das, R. Fierro, V. Kumar, J. P. Ostrowski, J. Spletzer, and C. J. Taylor, A vision-based formation control framework, *IEEE Trans. Robot. Autom.*, vol. 18, no. 5, pp. 813–825, 2002.

Zhenge Yang received the bachelor degree from Beijing Institute of Technology, China in 2021. He is currently pursuing the PhD degree with the School of Mechanical Engineering, Beijing Institute of Technology. His research directions are intelligent human-machine systems, brain-controlled intelligent vehicles, and brain-computer interface.

Weiming Chi received the master degree from Beijing Institute of Technology in 2022. His research interests include intelligent human-computer systems, brain-controlled intelligent vehicles, and brain-computer interfaces.

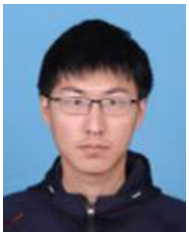

Haonan Shi received the bachelor degree from Beijing Institute of Technology, China in 2019. He is currently pursuing the PhD degree with the School of Mechanical Engineering, Beijing Institute of Technology. His research interests include brain-computer interface, brain-controlled vehicles, and intelligent human-machine system.

Luzheng Bi received the PhD degree in mechanical engineering from Beijing Institute of Technology, Beijing, China in 2004. From 2007 to 2008, he was a visiting scholar with the Department of Industrial and Operations Engineering, University of Michigan, Ann Arbor, MI, USA. From Nov. 2017 to May 2018, he was a visiting scholar with the Department of Computer Science and Engineering, Nanyang Technological University, Singapore. He is currently a professor and the director of the Institute of Mechatronic Systems, the School of Mechanical Engineering, Beijing Institute of Technology. His research interests include intelligent systems, brain-controlled robots and vehicles, human-machine collaboration, and human behavior modeling. He is an associate editor of *Complex System Modeling and Simulation*, *IEEE/ASME AIM*, *ASME DSCC*, *ACC*, and *CCC*. He is an author of refereed journal articles in the *IEEE Transactions on Cybernetics*, *IEEE Transactions on intelligent Transportation Systems*, *IEEE Transactions on Biomedical Engineering*, *IEEE Transactions on Neural Systems and Rehabilitation Engineering*, *IEEE Transactions on Systems*, *Man*, *and Cybernetics*, and other journals. He received the Natural Science Award by the Ministry of Education of China and Electronics and Information Science and Technology Award by the Chinese Society of Electronics. He was the recipient of the Supervisor Awards of Outstanding Doctoral Dissertation and Outstanding Master Thesis of the Beijing Institute of Technology.

Cuntai Guan is a president's chair professor in computer science and engineering at Nanyang Technological University (NTU), Singapore. He is the director of the Artificial Intelligence Research Institute (AI.R) of NTU. He is the co-director of S-Lab for Advanced Intelligence (S-Lab), NTU. He is the director of the Centre for Brain-Computing Research (CBCR). He is on the Steering Committee of Ageing Research Institute for Society and Education (ARISE), NTU. He is a member of the Management Committee of the Singapore Health Technologies Consortium (HealthTEC), Singapore. He serves on the Advisory Board of the Elite Master Program in Neuroengineering, TUM, Germany. He serves as the scientific advisor of several AI/BCI companies. He initiated and served as the co-director of the Rehabilitation Research Institute of Singapore (RRIS) from 2015 to 2018. Prior to joining NTU in 2016, he was the founding department head of the Neural & Biomedical Technology Department and Principal Scientist II (RSE6) at the Institute for Infocomm Research (I2R), Agency for Science, Technology, and Research (A*SATR), Singapore. He is an elected fellow of the Singapore Academy of Engineering (SAEng), the Institute of Electrical and Electronics Engineers (IEEE), and the American Institute for Medical and Biological Engineering (AIMBE). His research interests are in the fields of brain-computer interfaces (BCI), machine learning, neural signal & image processing, data analytics, and artificial intelligence. He published 7 book chapters and 370 refereed journal and conference papers, and held 25 granted patents and patent applications. He licensed 15 patents/technologies to five companies in Singapore and USA. He delivered more than 70 keynote speeches and invited talks (including the keynote, Brain-Computer Interfaces for Stroke Rehabilitation, at the opening ceremony of the 7th International BCI Meeting, Asilomar, USA, May 2018). He is a recipient of the Annual BCI Research Award, the IES Prestigious Engineering Achievement Award, Achiever of the Year (Research) Award, Finalist of President Technology Award, and winner of BCI Competitions. He has been an associate editor for *IEEE Transactions on Biomedical Engineering*, *IEEE Transactions on Artificial Intelligence*, *Pattern Recognition*, *Neurocomputing*, *Brain-Computer Interfaces*, *Frontiers in Neuroscience*, *Frontiers in Human Neuroscience*, *A*STAR Research Publication*, and the guest-editor for *IEEE Computational Intelligence Magazine*. He is on the Advisory Board of *IEEE Open Access Journal of Engineering in Medicine and Biology* (*OJEMB*). He was on the IEEE Fellow Evaluation Committee for EMBS Society, 2018 and 2020. He was an APSIPA Distinguished Lecturer, 2017 and 2018. He served as the general co-chair for IEEE ICAA'2018, conference chair for the Internet of Things (IoT) Asia 2015, and general chair for the IEEE HealthCom 2008. He was the president of Pattern Recognition and Machine Intelligence Association (PREMIA), Singapore, from 2008 to 2010.